Supplement of Atmos. Chem. Phys., 21, 16257–16276, 2021
https://doi.org/10.5194/acp-21-16257-2021-supplement

Atmospheric Chemistry and Physics
Open Access

Supplement of

Atmospheric observations consistent with reported decline in the UK's methane emissions (2013–2020)

Mark F. Lunt et al.

Correspondence to: Mark F. Lunt (mark.lunt@ed.ac.uk)

List of Figures

1 Supplementary Figures

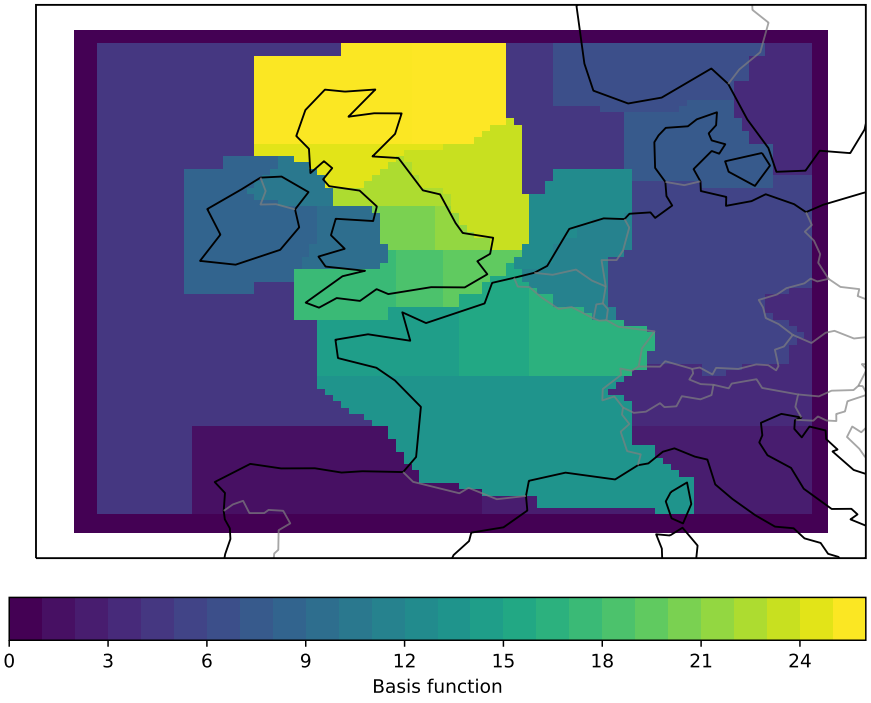

Figure S1. Arrangement of the fixed spatial basis functions used in the GEOS-Chem inversions.

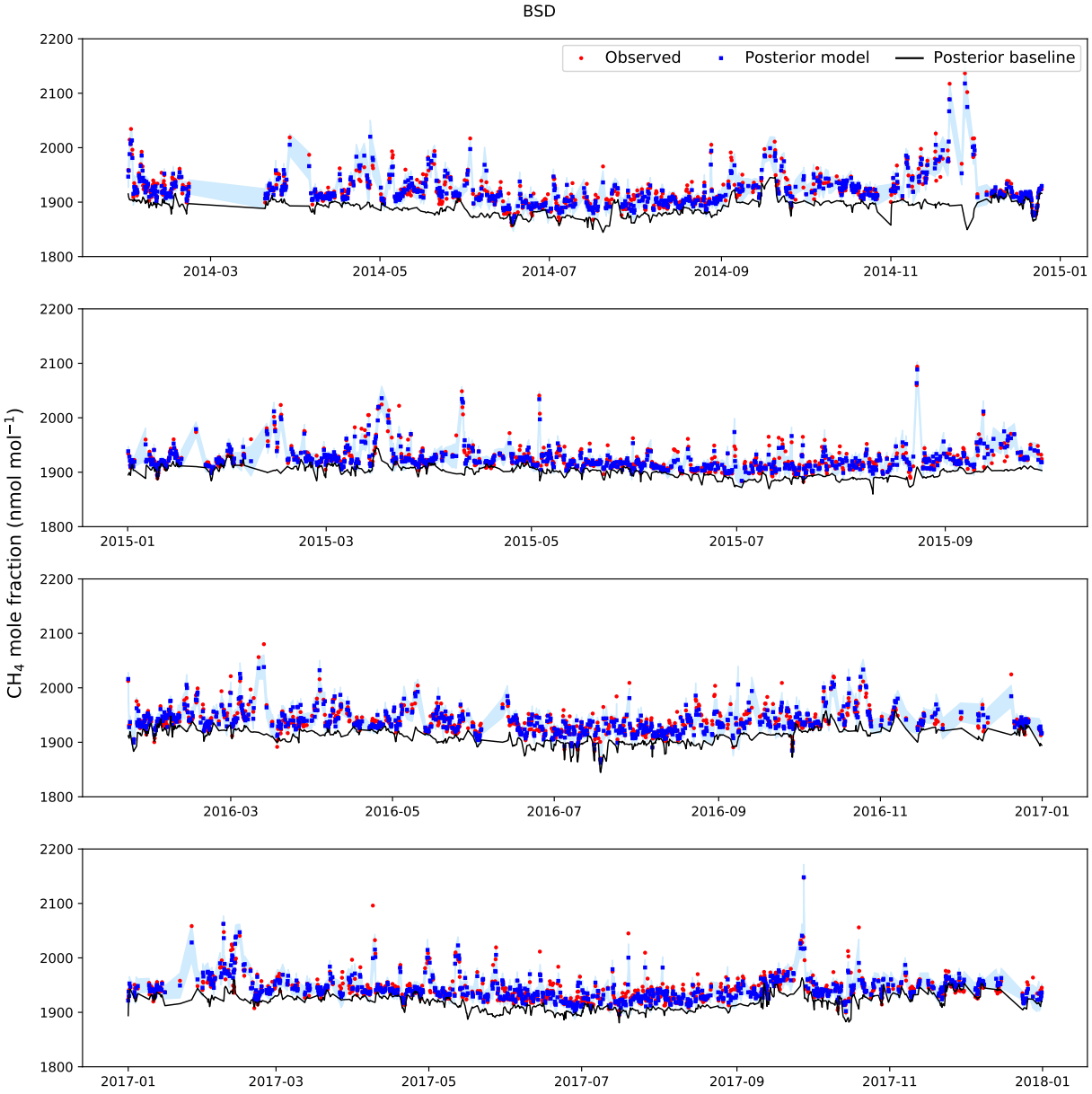

Figure S2. Observed (red) and modelled mole fractions (blue) at BSD between 2014–2017. The posterior modelled baseline is shown in black. Shading represents the posterior model-measurement uncertainty.

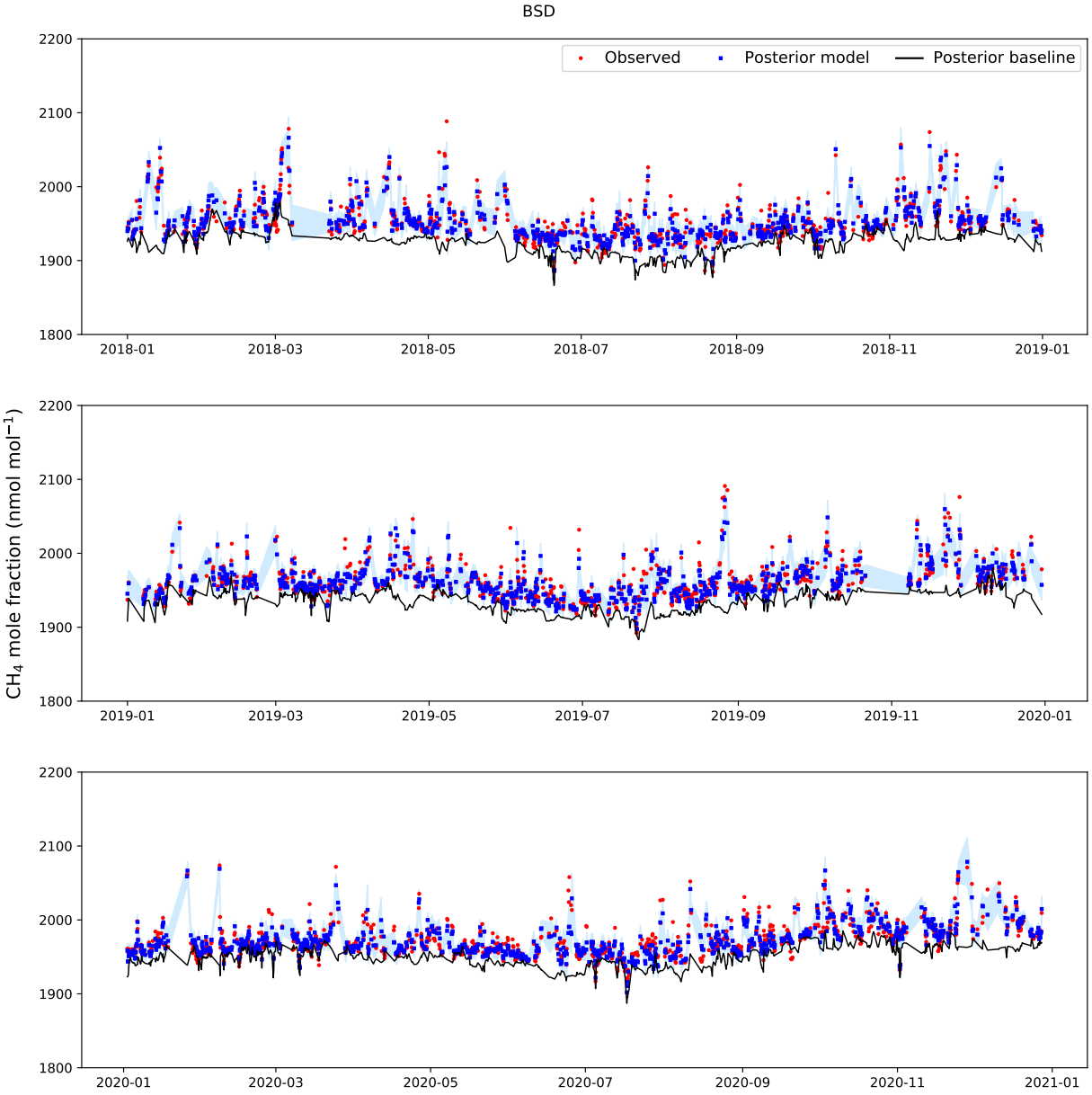

Figure S3. Observed (red) and modelled mole fractions (blue) at BSD between 2018–2020. The posterior modelled baseline is shown in black. Shading represents the posterior model-measurement uncertainty.

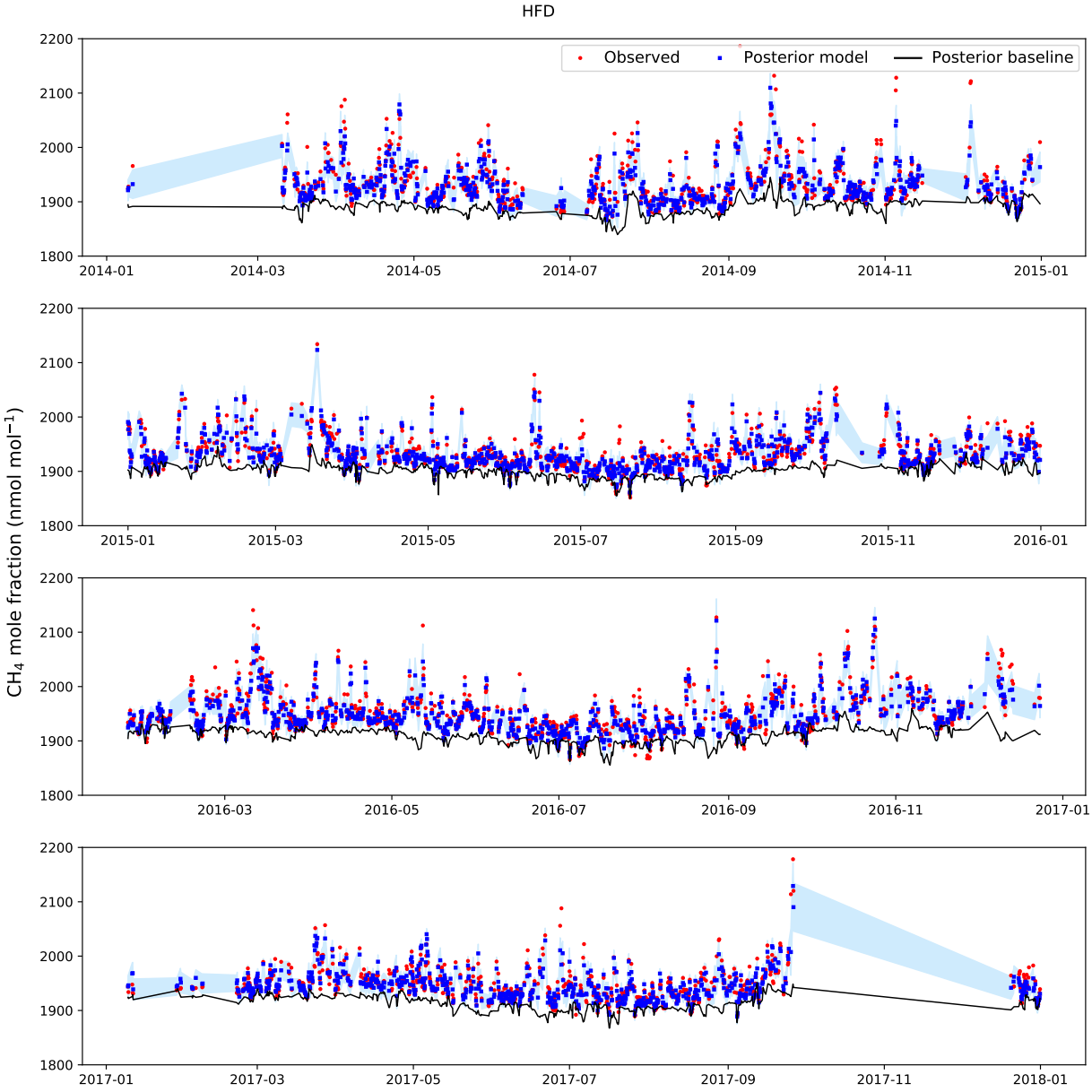

Figure S4. Observed (red) and modelled mole fractions (blue) at HFD between 2014–2017. The posterior modelled baseline is shown in black. Shading represents the posterior model-measurement uncertainty.

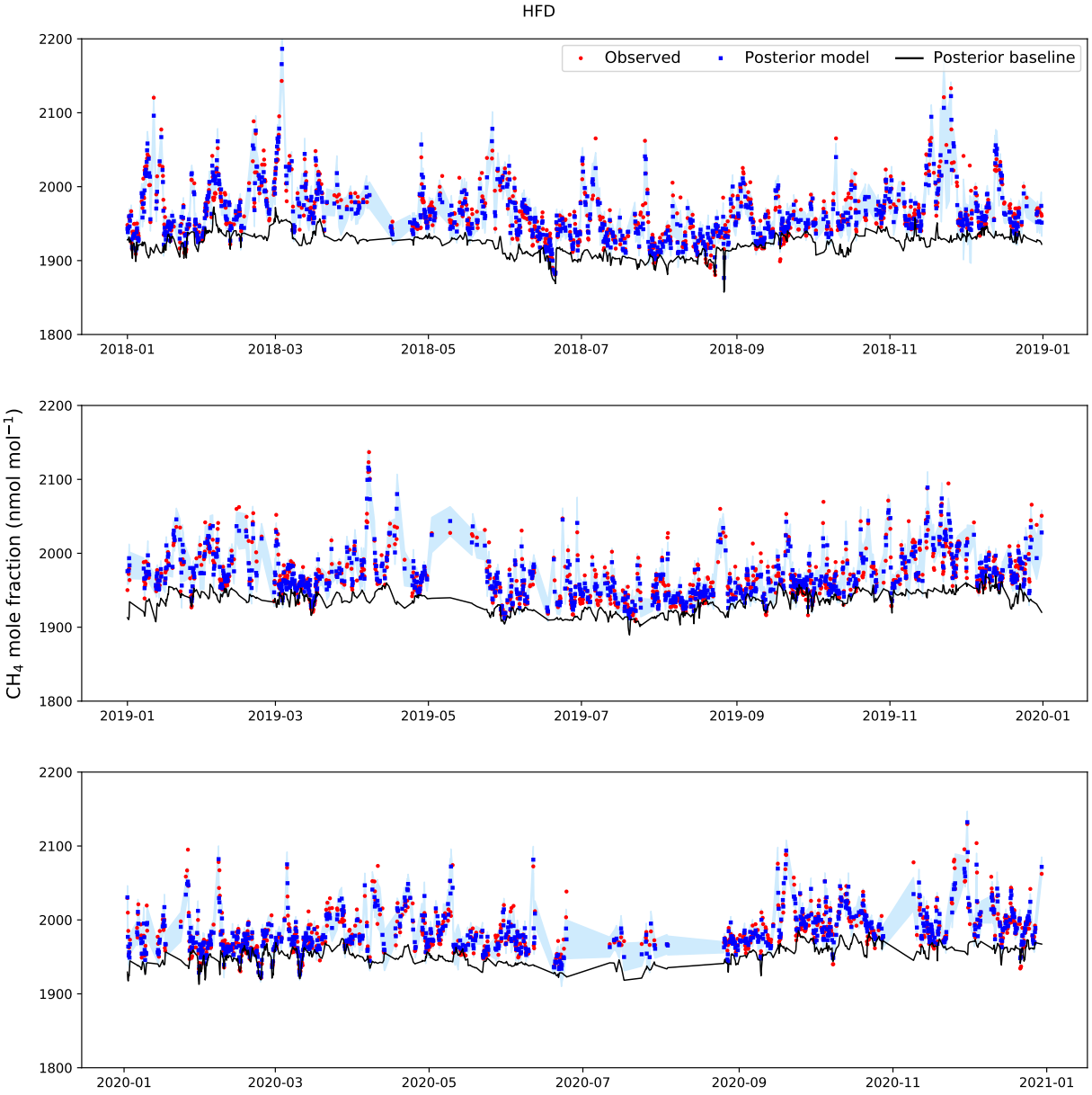

Figure S5. Observed (red) and modelled mole fractions (blue) at HFD between 2018–2020. The posterior modelled baseline is shown in black. Shading represents the posterior model-measurement uncertainty.

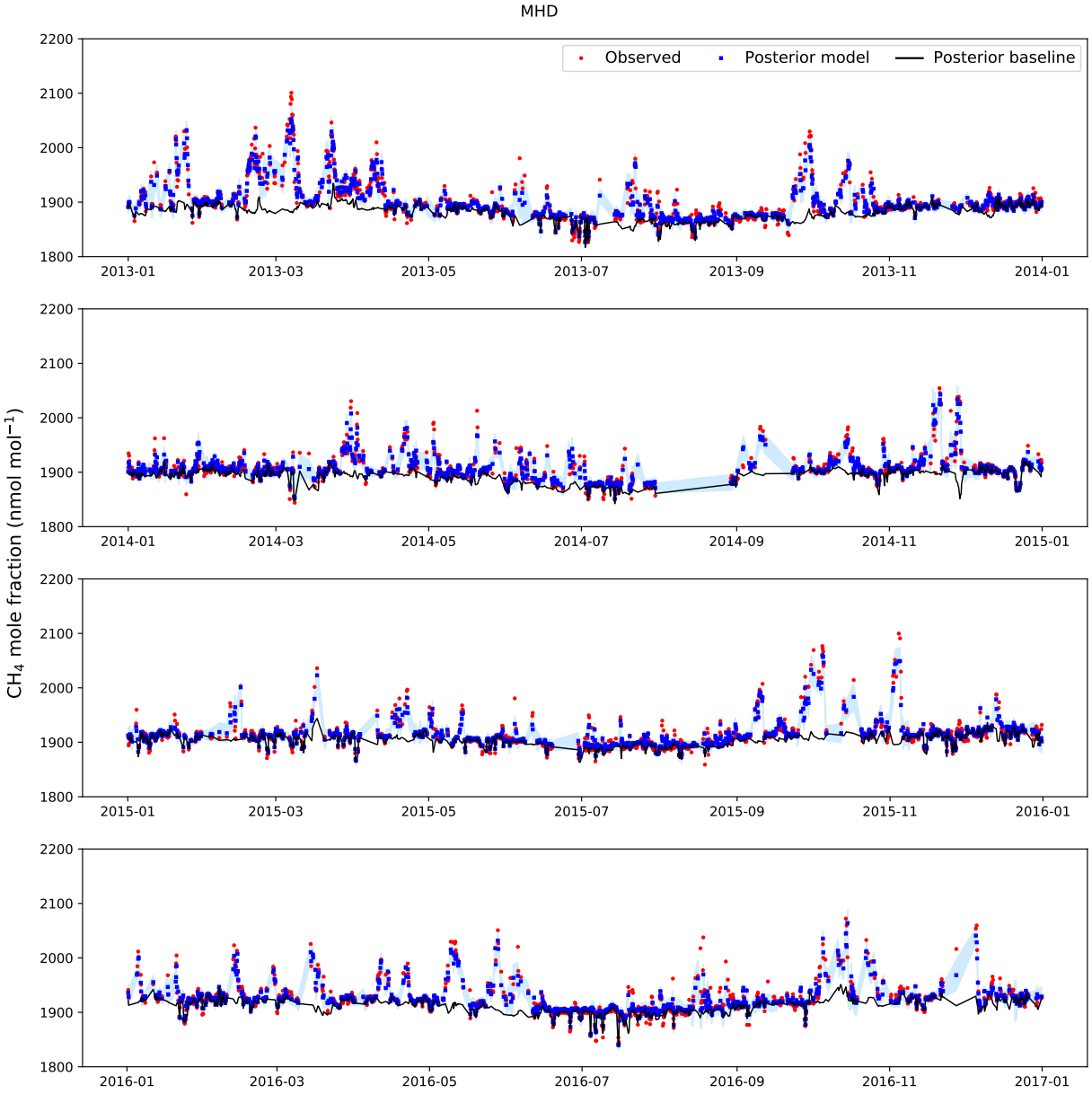

Figure S6. Observed (red) and modelled mole fractions (blue) at MHD between 2013–2016. The posterior modelled baseline is shown in black. Shading represents the posterior model-measurement uncertainty.

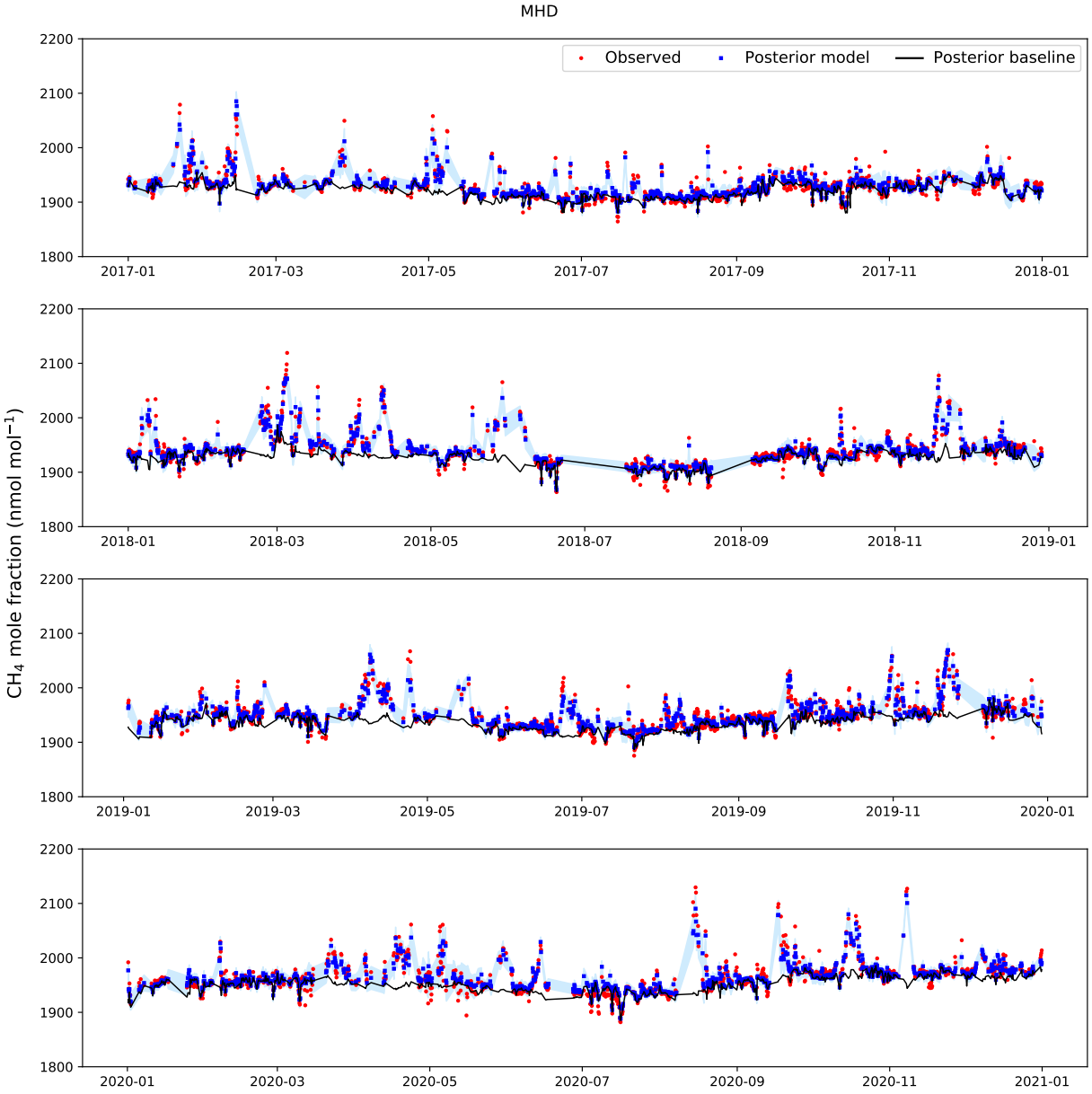

Figure S7. Observed (red) and modelled mole fractions (blue) at MHD between 2017–2020. The posterior modelled baseline is shown in black. Shading represents the posterior model-measurement uncertainty.

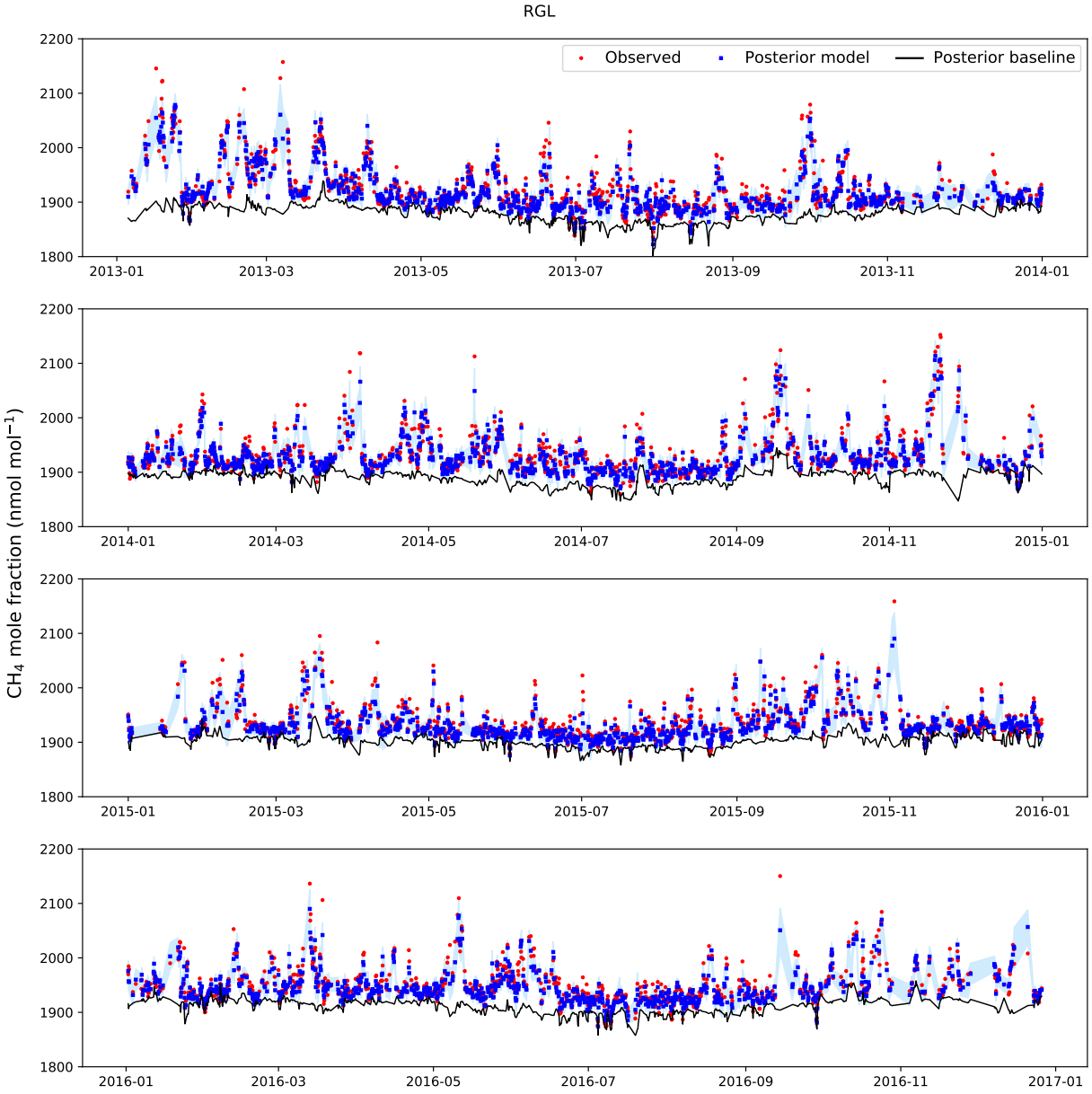

Figure S8. Observed (red) and modelled mole fractions (blue) at RGL between 2013–2016. The posterior modelled baseline is shown in black. Shading represents the posterior model-measurement uncertainty.

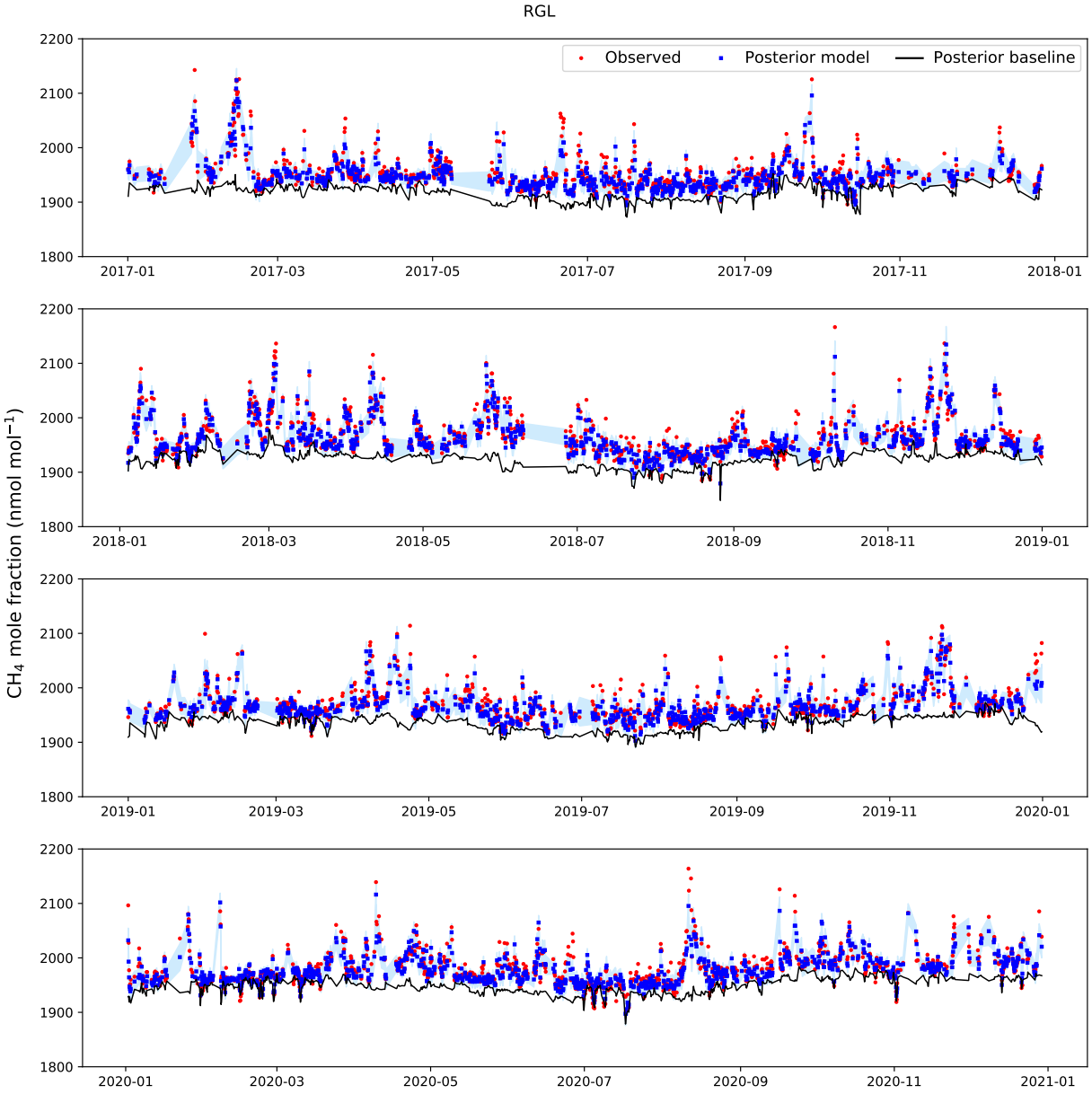

Figure S9. Observed (red) and modelled mole fractions (blue) at RGL between 2017–2020. The posterior modelled baseline is shown in black. Shading represents the posterior model-measurement uncertainty.

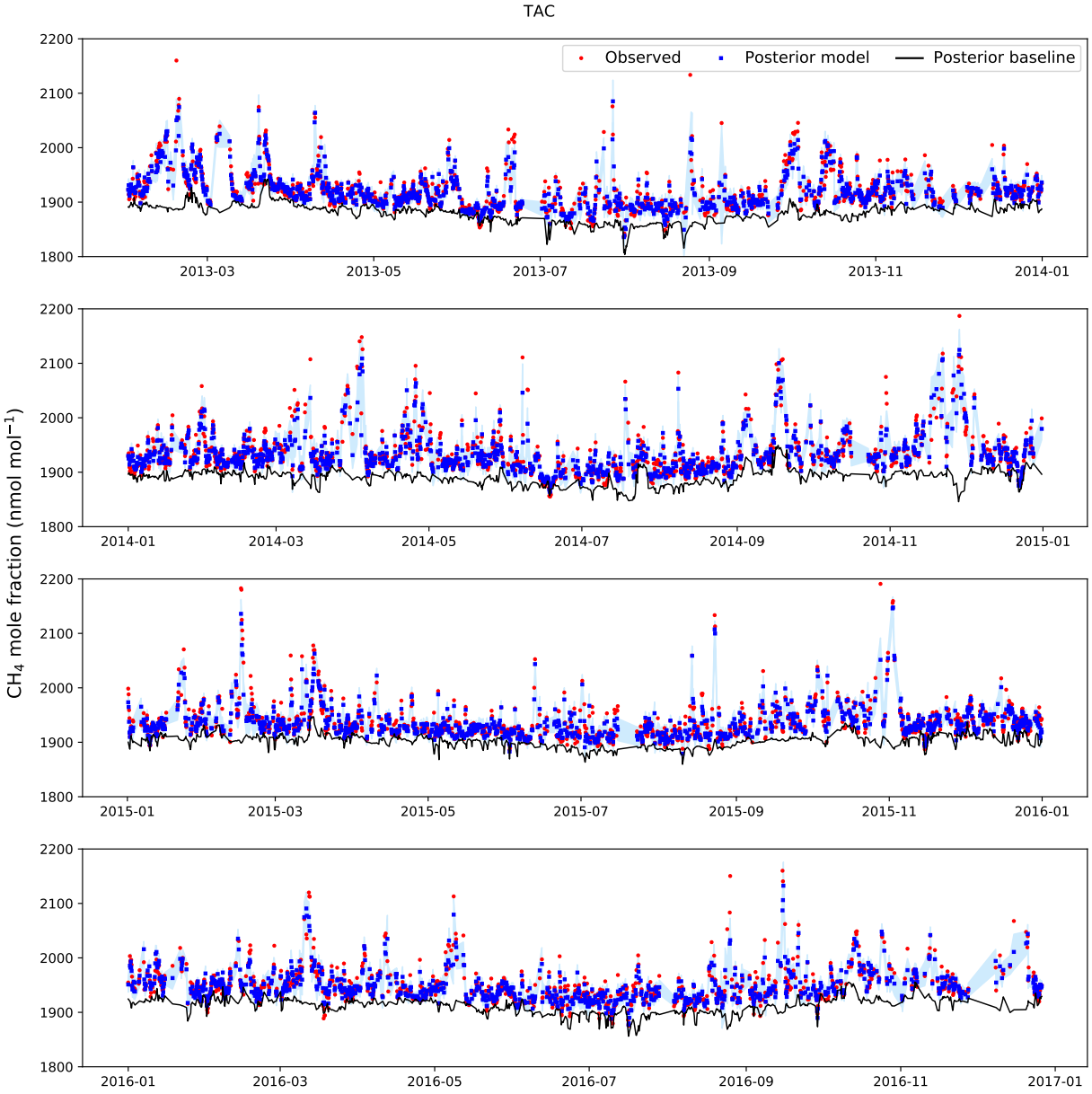

Figure S10. Observed (red) and modelled mole fractions (blue) at TAC between 2013–2016. The posterior modelled baseline is shown in black. Shading represents the posterior model-measurement uncertainty.

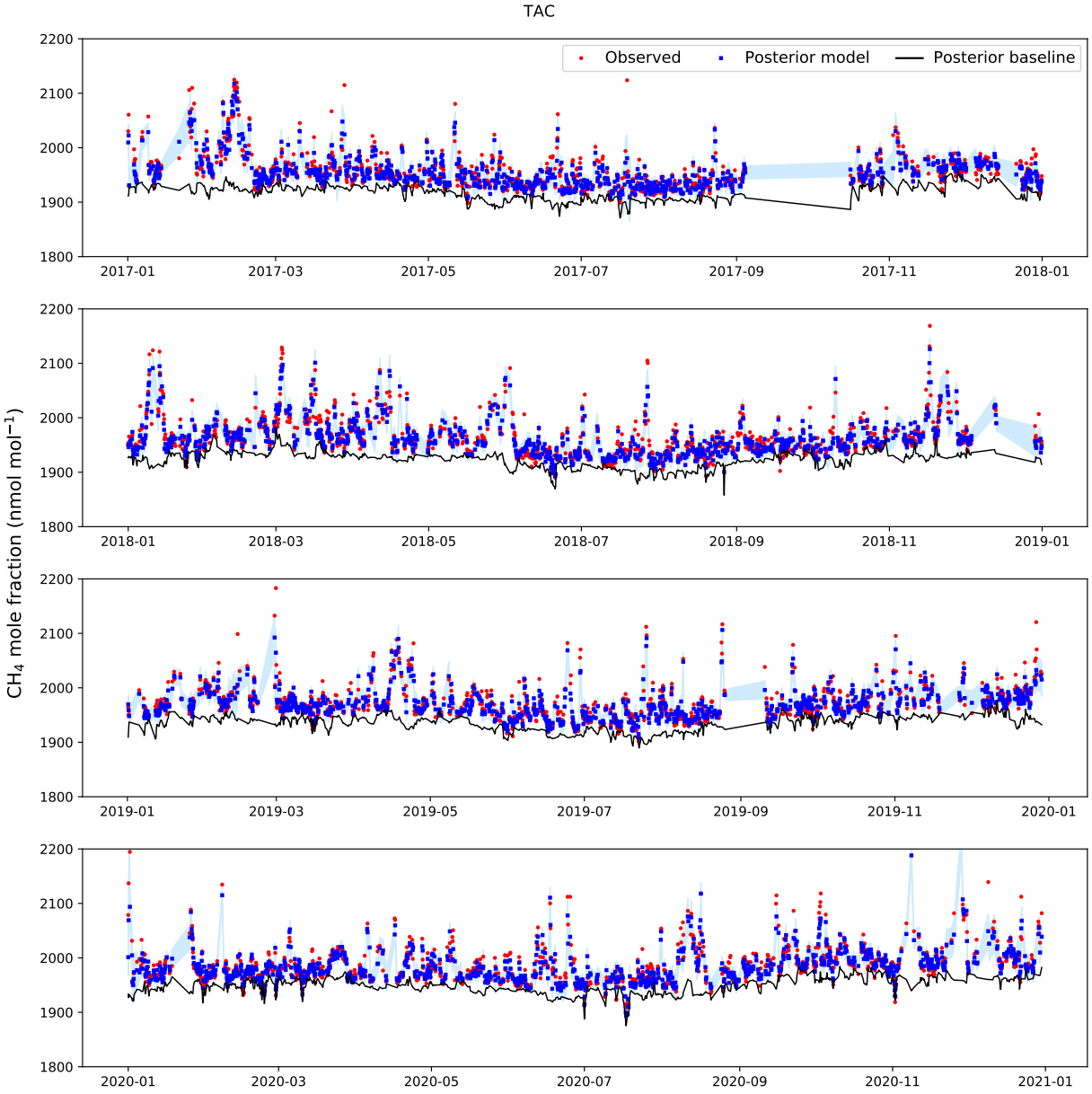

Figure S11. Observed (red) and modelled mole fractions (blue) at TAC between 2017–2020. The posterior modelled baseline is shown in black. Shading represents the posterior model-measurement uncertainty.

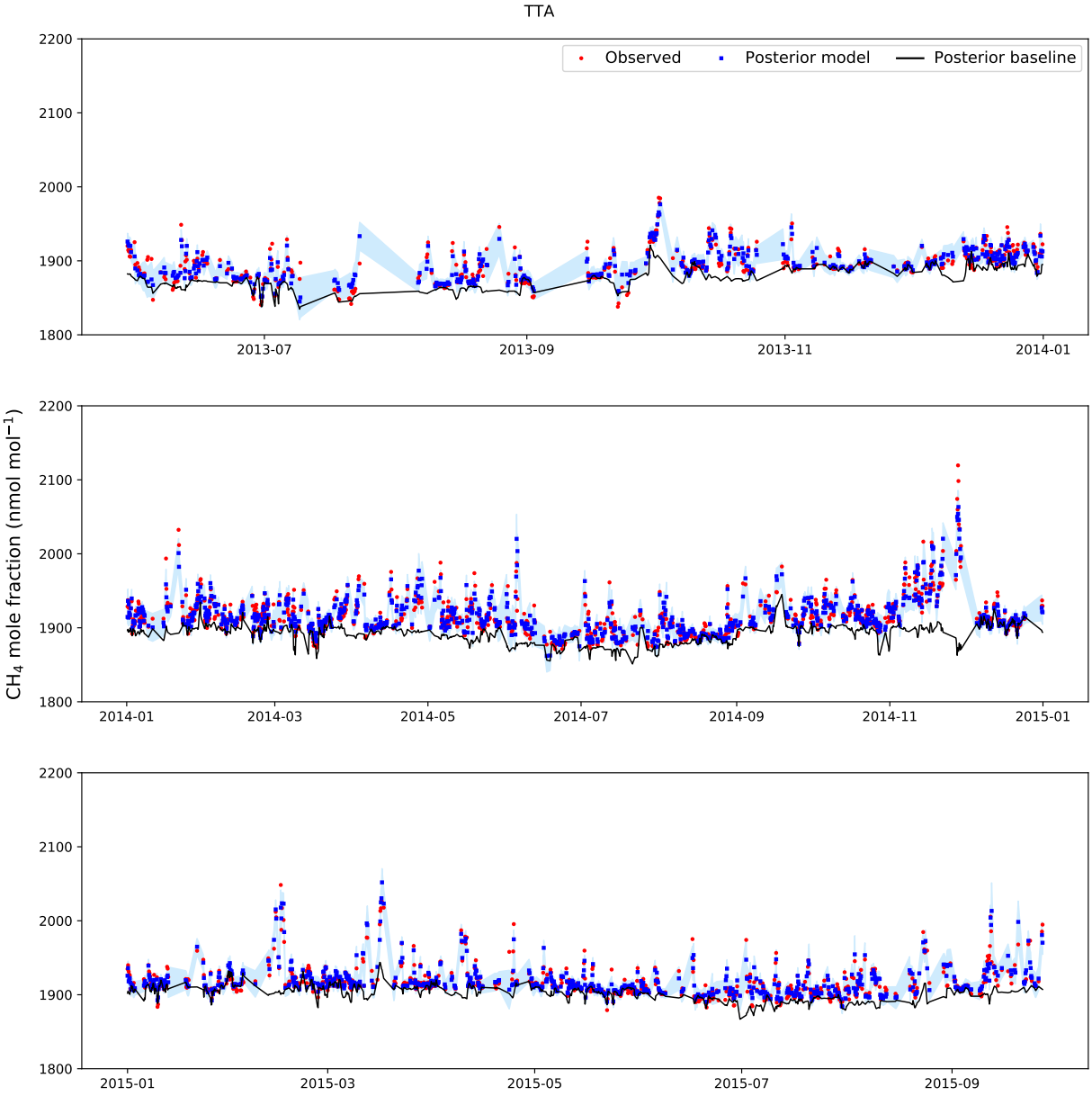

Figure S12. Observed (red) and modelled mole fractions (blue) at TTA between 2013–2015. The posterior modelled baseline is shown in black. Shading represents the posterior model-measurement uncertainty.

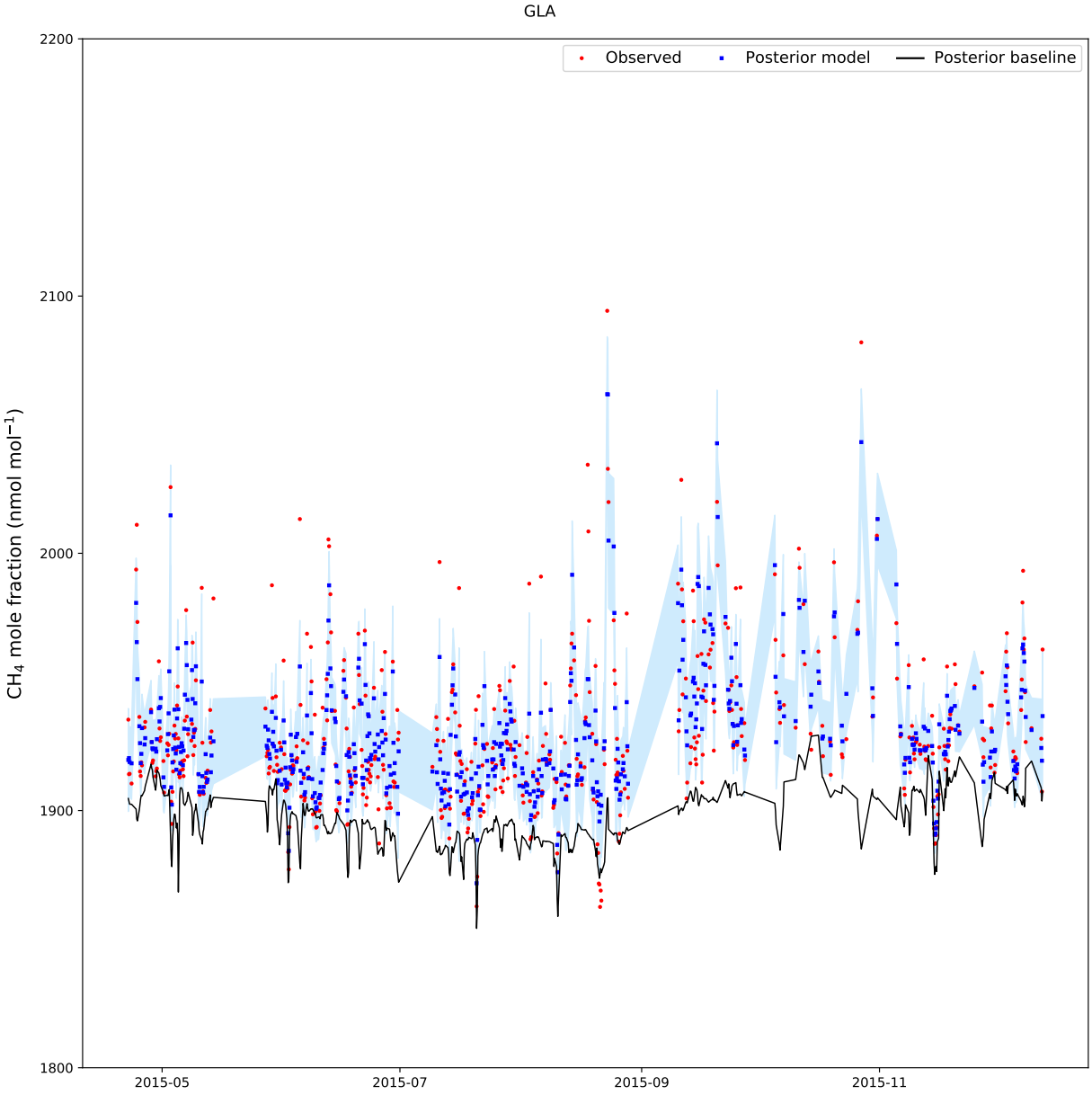

Figure S13. Observed (red) and modelled mole fractions (blue) at GLA during 2015. The posterior modelled baseline is shown in black. Shading represents the posterior model-measurement uncertainty.

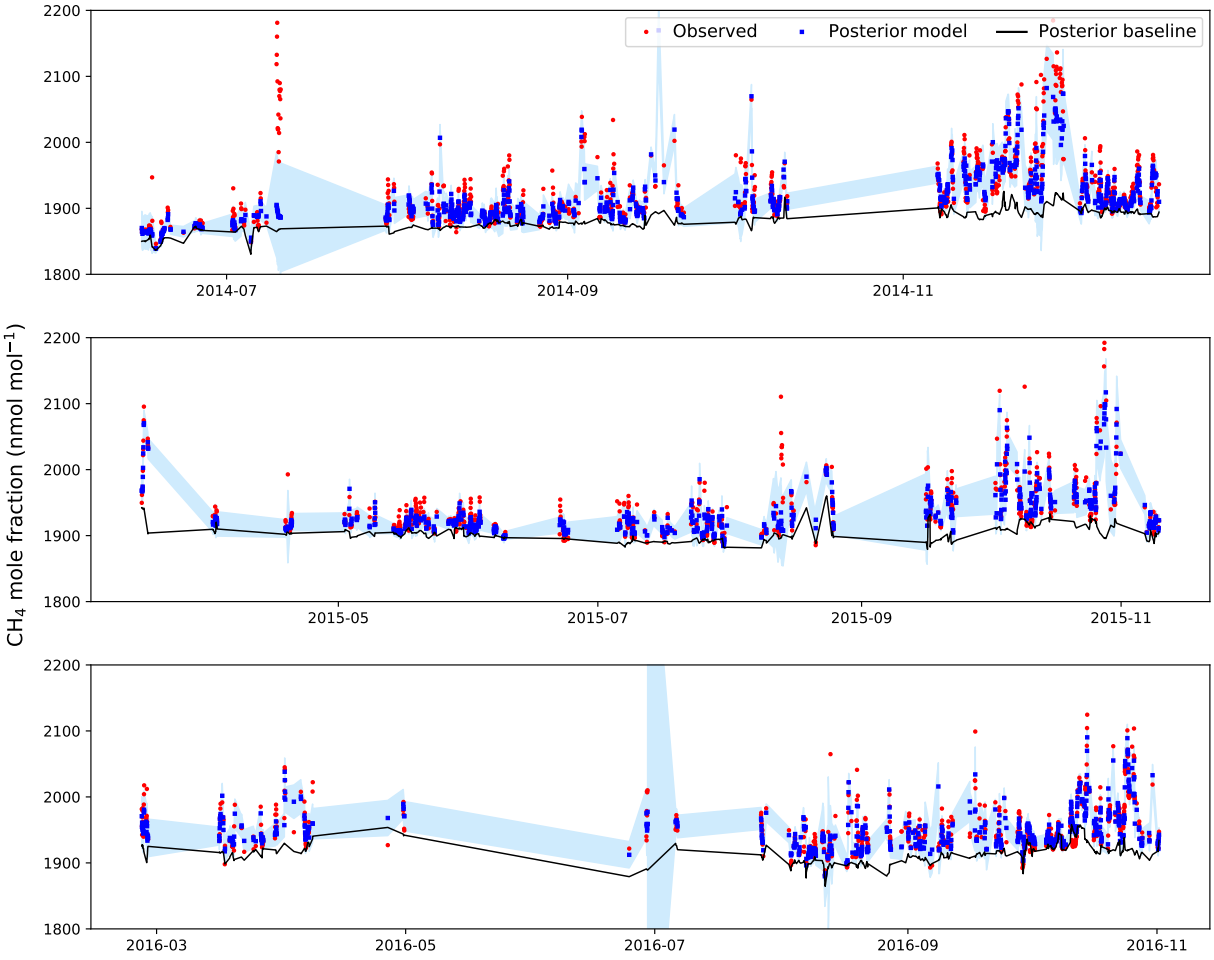

Figure S14. Observed (red) and modelled mole fractions (blue) from the DFDS ferry between 2014–2016. The posterior modelled baseline is shown in black. Shading represents the posterior model-measurement uncertainty.

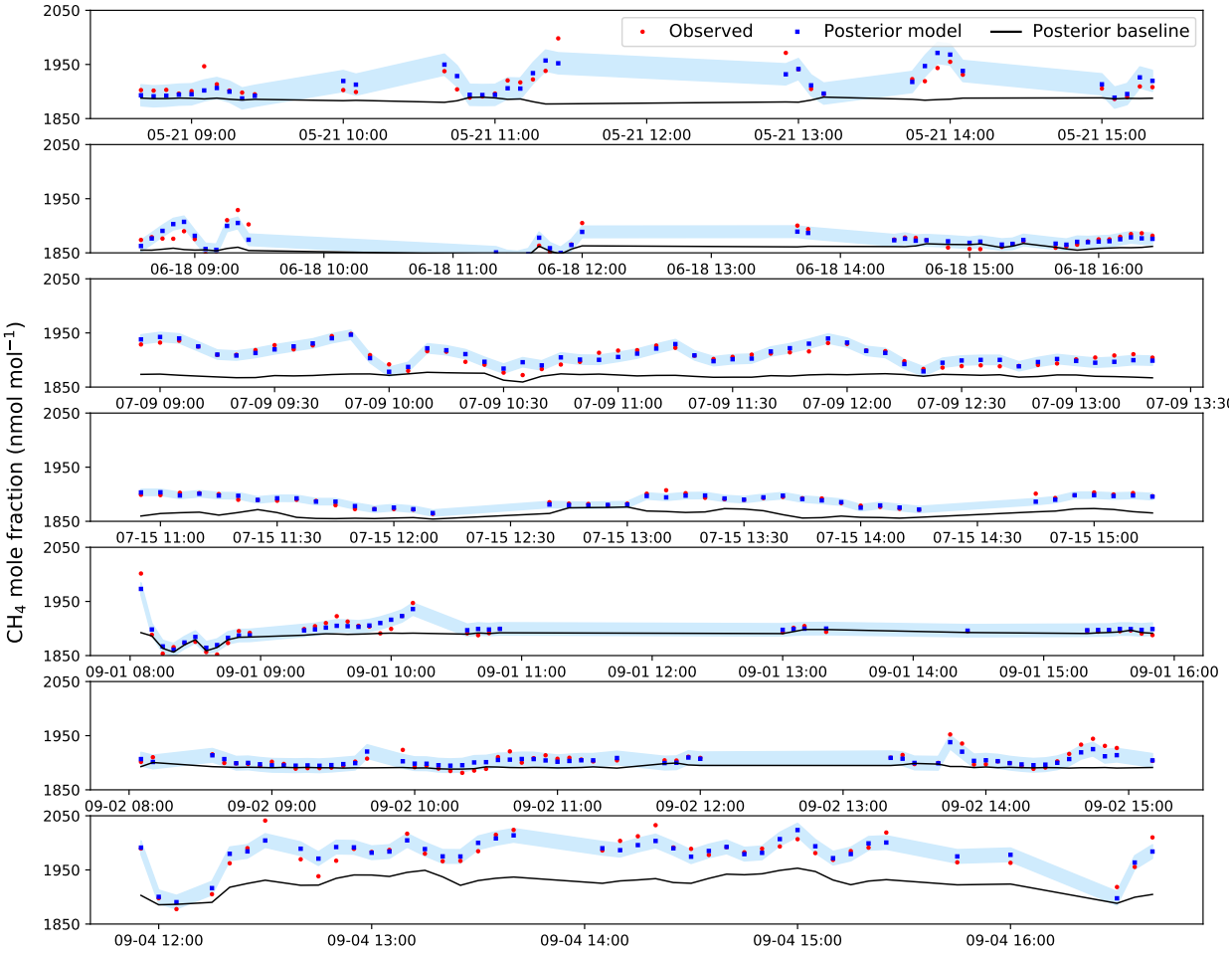

Figure S15. Observed (red) and modelled mole fractions (blue) from the FAAM aircraft during 2014. The posterior modelled baseline is shown in black. Shading represents the posterior model-measurement uncertainty.

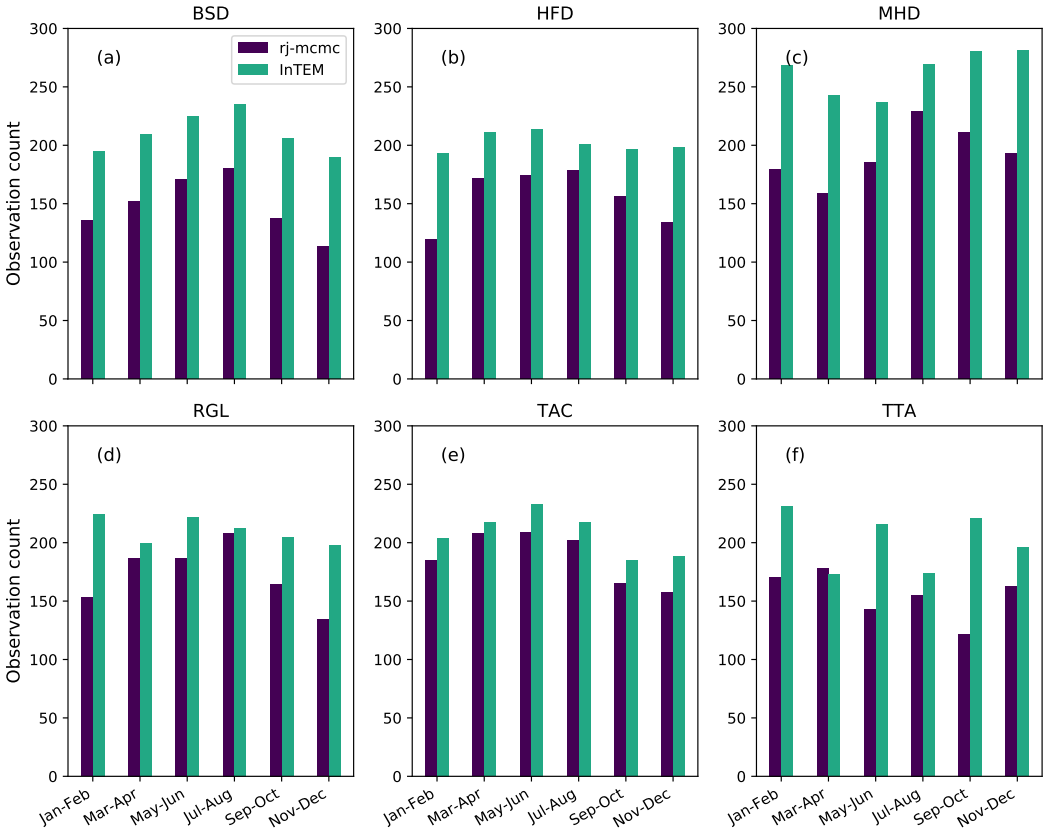

Figure S16. Number of 4-hour average observations used in the rj-mcmc and InTEM inversions at each site per 2-month period. 2-monthly counts are the average in each 2-month period across all years.

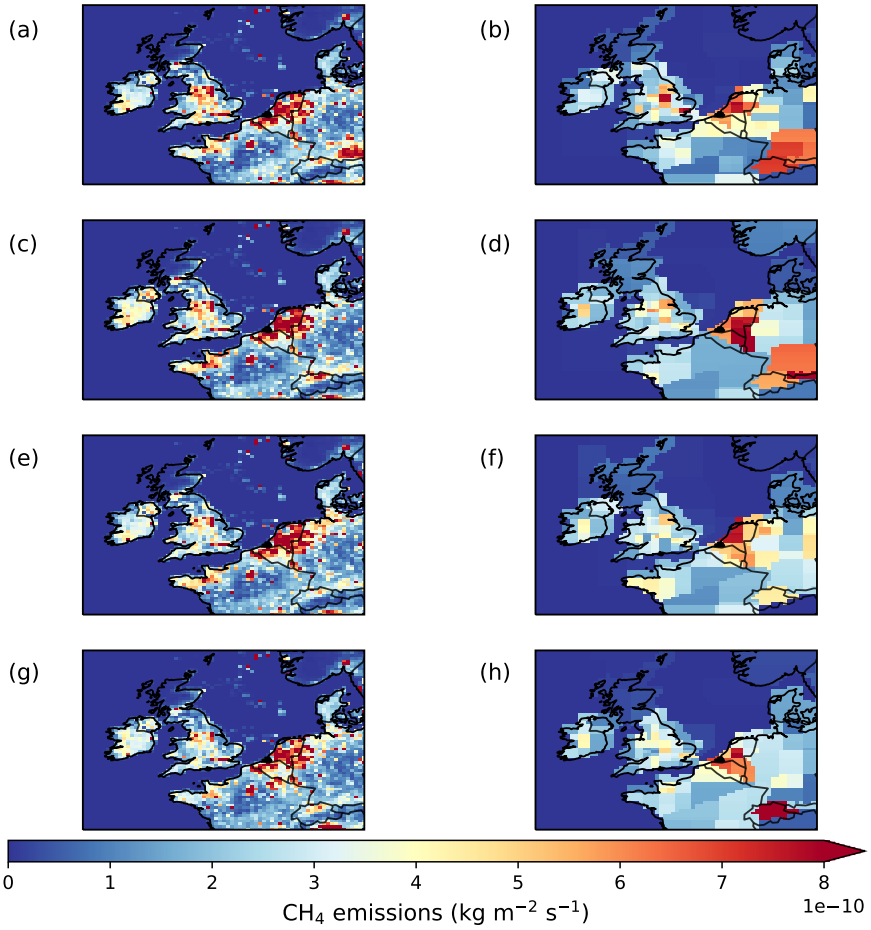

Figure S17. Posterior annual mean emissions distribution from rj-mcmc and InTEM inversions. The left column shows the rj-mcmc distributions and the right column InTEM for (a)–(b) 2014, (c)–(d) 2016, (e)–(f) 2018, (g)–(h) 2020.

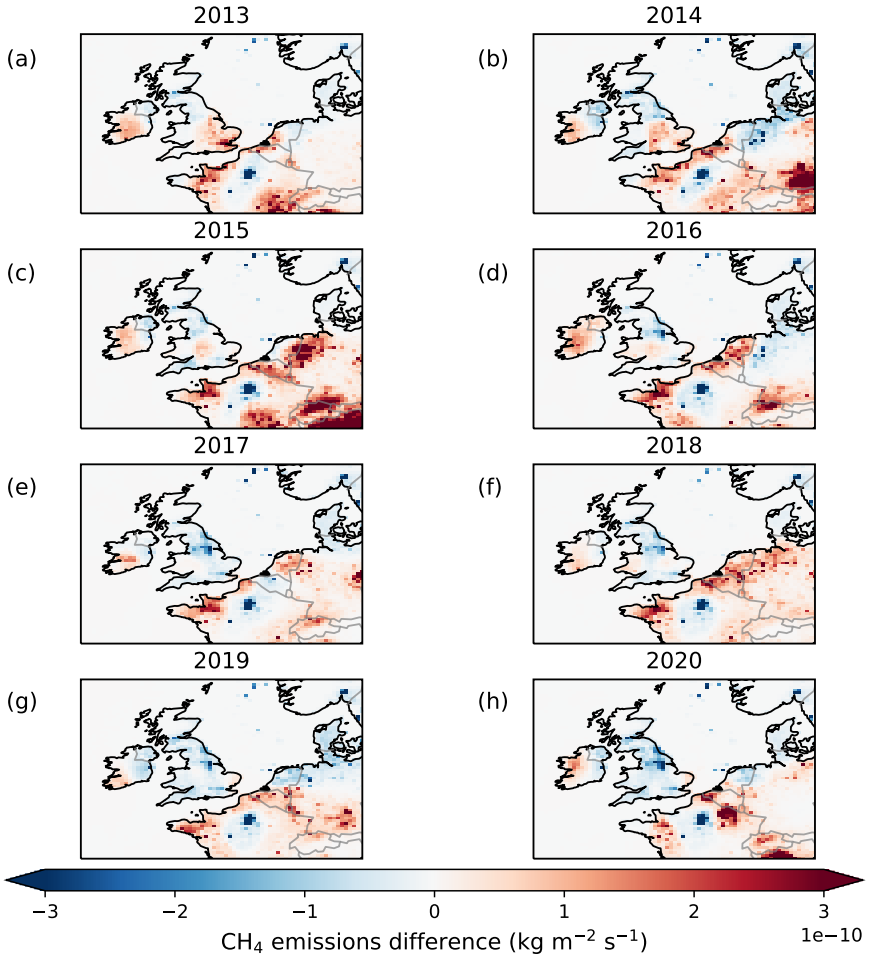

Figure S18. Annual mean emissions difference between the posterior and prior distributions from the rj-mcmc inversions between 2013–2020.

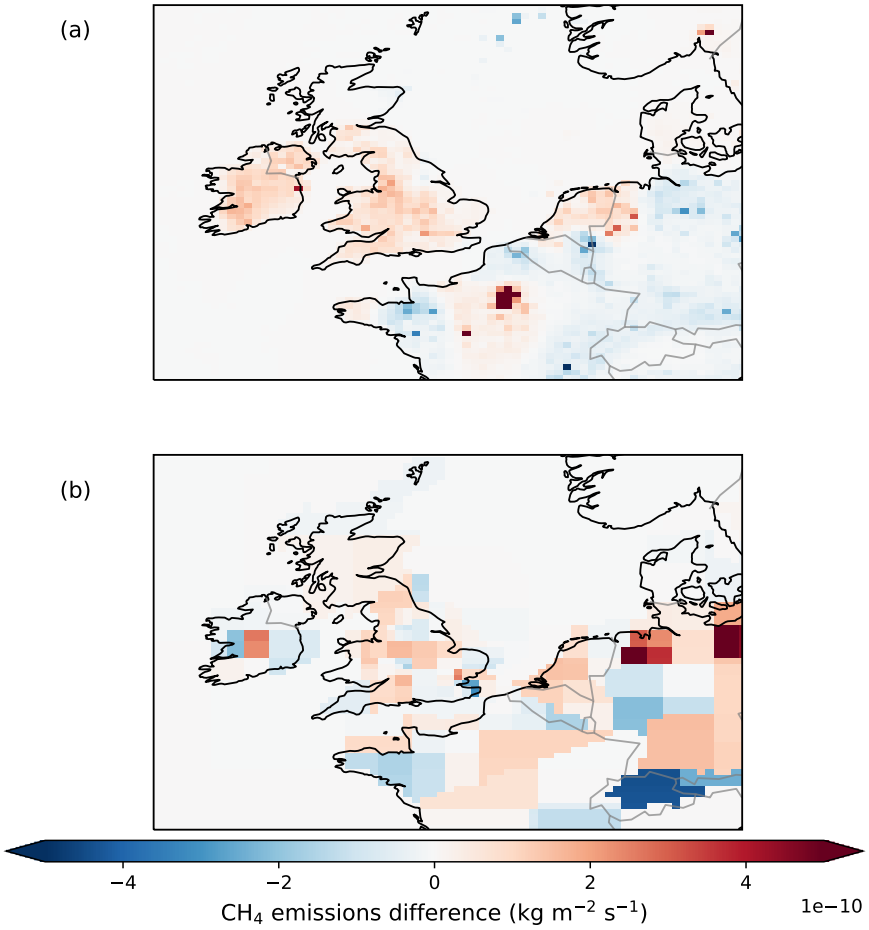

Figure S19. Posterior distribution of the summer 2018 (May–August) anomaly from the 2018 posterior mean emissions from (a) the rj-mcmc and (b) InTEM inversions. The distribution show the positive anomaly over the UK was fairly uniformly distributed and primarily from central and western areas.

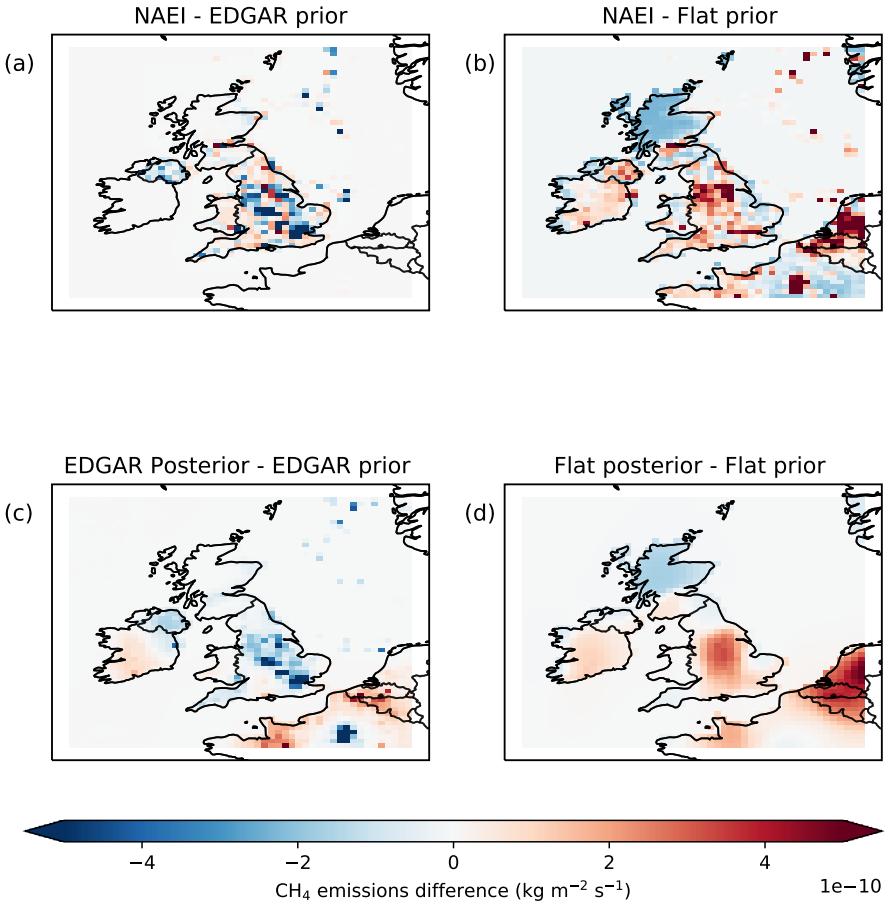

Figure S20. Maps of the differences between the different prior distributions and the respective posteriors. (a) the difference between the NAEI prior and EDGAR; (b) the difference between the NAEI and flat prior; (c) posterior mean from the EDGAR prior inversion minus EDGAR prior; (d) posterior mean from the flat prior inversion minus flat prior. The posterior differences are broadly similar to the differences between the NAEI and the respective priors.

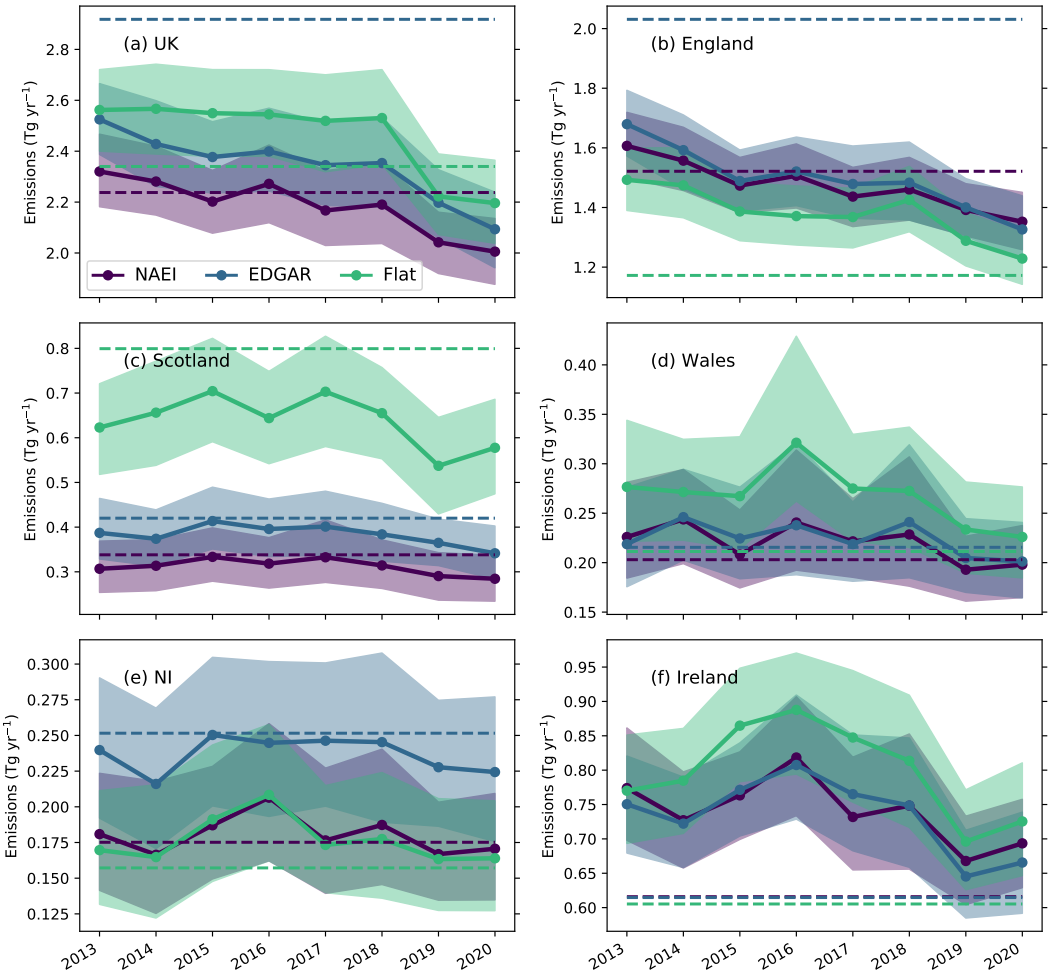

Figure S21. Annual mean emissions between 2013–2020 for MHD-TAC inversions using different prior distributions from the NAEI (purple), EDGAR (blue) and a flat distribution (green). Estimates are shown for (a) the UK, (b) England, (c) Scotland, (d) Wales, (e) NI and (f) Ireland. Shading represents the 95% confidence interval. Dashed lines represent the magnitudes of the respective priors.